JOURNAL OF GEOPHYSICAL RESEARCH, VOL. 97, NO. D1, PAGES 899-916, JANUARY 20, 1992

Atmospheric Water Vapor Measurements: Comparison of Microwave Radiometry and Lidar

MARTIN N. ENGLAND[1]

Interferometrics Inc., Vienna, Virginia

R. A. FERRARE

Universities Space Research Association, Washington, D.C.

S. H. MELFI

Laboratory for Atmospheres, NASA/GSFC, Greenbelt, Maryland

D. N. WHITEMAN, T. A. CLARK

Laboratory for Terrestrial Physics, NASA/GSFC, Greenbelt, Maryland

The NASA/GSFC Crustal Dynamics Project microwave water vapor radiometer (J03) is evaluated in terms of measurements of the integrated precipitable water vapor content of a particular column of the troposphere. The measurements were taken during the Atmospheric Moisture Intercomparison Study (ATMIS) held at Wallops Island, Virginia, during April 1989. Various water vapor sensing instruments were used during ATMIS, including radiometers, radiosondes, and the NASA/GSFC Raman lidar. Comparisons between water vapor measurements by the radiometer and the lidar yielded a correlation coefficient of 0.998 and rms differences for three nights of -0.2 ± 0.2 mm (April 11-12, 1989), -0.8 ± 0.5 mm (April 16-17, 1989), and -0.4 ± 0.3 mm (April 17-18, 1989). The integrated precipitable water vapor measurements for these three nights were approximately 5, 10, and 21 mm, respectively. The first two periods had clear meteorological conditions, while clouds were present during the third period. The lidar results during the third period are augmented with radiosonde measurements above the cloud base. This study shows that the radiometer provides accurate, continuous measurements of the water vapor integrated through the depth of the atmosphere.

1. INTRODUCTION

The Crustal Dynamics Project (CDP) at NASA/Goddard Space Flight Center utilizes very long baseline interferometry (VLBI) to measure tectonic plate motions worldwide by observing extragalactic radio sources (quasars) [*Clark et al.*, 1985]. The observed signal electrical path length error due to tropospheric constituents is a major error source in measuring the components of an observing station's position [e.g., *Shapiro*, 1976; *Resch*, 1980; *Clark et al.*, 1985; *Elgered et al.*, 1991]. The extra signal delay introduced by the troposphere is usually separated into two terms: the hydrostatic (or "dry") term and the "wet" term [*Davis et al.*, 1985]. The "wet" term is dominated by the dipole component of the water vapor refractivity, while the "dry" term is dominated by O_2 and N_2 and the nondipole component of water vapor refractivity. As a result the "dry" term can be estimated from the barometric pressure. Profiles of meteorological quantities such as temperature, pressure and humidity can be measured in situ by radiosondes, and the water vapor content derived from these measurements. However, this method is costly and time-consuming, and the path of the balloon cannot be controlled. It is well known that the amount of water vapor in the troposphere is related to the thermal emission near the 22.235 GHz (1.35 cm) spectral line [e.g. *Dicke et al.*, 1946]. Consequently, the CDP is investigating the use of ground-based microwave radiometers to measure tropospheric brightness temperatures and from these derive the integrated water vapor content of the troposphere and the associated "wet" portion of the delay.

The "fundamental" quantities produced by the J series microwave water vapor radiometer (WVR) are measurements of the line-of-sight brightness temperatures at three frequencies, 20.7, 22.2, and 31.4 GHz (wavelengths, λ, of 1.45, 1.35, and 0.95 cm). The brightness temperatures are converted into opacities at these frequencies and combined to produce estimates, via the use of a retrieval algorithm, of the integrated precipitable water vapor content of that particular column of the atmosphere. Because the performance of the WVR in measuring the absolute brightness temperatures is critical for subsequent VLBI data reduction, some method is needed to calibrate the absolute performance of the instrument. Since calibration of the WVR in the laboratory under "known" conditions is not feasible, the absolute performance must be calibrated by colocation experiments involving a variety of techniques, e.g., similar and different designs of radiometers, radiosondes, and Raman lidar systems. Various comparisons have been made between different types of instruments [e.g., *Elgered et al.*, 1982; *Heggli et al.*, 1987; *Askne et al.*, 1987; *Westwater et al.*, 1989]. The brightness temperature performance of the WVR can be investigated by comparing different types of radiometers and, by assuming a water vapor emission line model, by comparing with radiosonde data. The integrated water vapor measurements can be compared with Raman lidar measurements. A comparison between a Raman lidar system and a WVR has been made by *Askne et al.* [1987] during the Onsala Atmospheric Measurement (ONSAM) experiment. However, due to problems with this experiment, the

[1]Now at Computer Sciences Corporation.

Paper number 91JD02384.
0148-0227/92/91JD-02384$05.00

number and quality of the humidity profiles obtained were limited, which reduced the usefulness of the experiment. The lidar signals for the ONSAM experiment were fairly clean between 50 and 550 m, and the large-scale correlation between the radiosonde profiles and the lidar profiles was good with the differences being attributed to a slow humidity detector in the radiosonde or to the fact that the two instruments measure different volumes.

An opportunity to compare the integrated water vapor measurements from the CDP WVR J03 with those from the GSFC Raman lidar system was available during the Atmospheric Moisture Intercomparison Study (ATMIS) held at Wallops Island, Virginia, from April 11, 1989, to April 18, 1989. The lidar and WVR use completely independent techniques, and thus an intercomparison between the two water vapor measurements could give valuable insight into the performance of the WVR, particularly in estimating the magnitude of systematic errors in the WVR system.

2. Water Vapor Radiometer Measurements

WVR System

The radiometer used in this experiment is a three channel microwave instrument operating at frequencies around the water vapor spectral line centered at 22.235 GHz (λ = 1.35 cm). The basic design of the instrument is described by *Janssen* [1985]. The addition of a "hot" load to the system has greatly improved the system calibration and allows better gain stability during periods when the meteorological conditions are not suitable for calibration (discussed below). The instrument is fully steerable in both azimuth and elevation, allowing full sky coverage to be obtained. A block diagram of the microwave package and the controlling hardware for the WVR system as configured for the ATMIS experiment is shown in Figures 1*a* and 1*b*. The incoming radiation passes through a frequency diplexer which splits the signal into channels 1 and 2 (20.7 and 22.7 GHz) and channel 3 (31.4 GHz). The hot load and a reference load are coupled into each of the microwave paths by ferrite switches, allowing the waveguide termination to be switched between the sky and the reference and hot loads. The signal is mixed down to an intermediate frequency with a passband of 40 - 200 MHz, amplified and detected by a square-law detector. Channels 1 and 2 share the same microwave circuit, differing only in the Gunn oscillator used in the mixing stage. The square-law detector output is amplified and converted (using a V/F counter) to a digital signal, which is passed to the data acquisition electronics to be logged as "counts" in the field data log. An estimate of the uncertainty on the count measurements is also logged in the field data log. Each logged measurement utilizes five repetitions of the switching sequence. Each switching sequence cycles through all the required combinations of the switches with blanking times inserted where appropriate to avoid switching transients (details are described by *Janssen* [1985]. Also included with each logged measurement is the output from an analog to digital (A/D) converter, which is dedicated to measuring thermistor voltages for temperature monitoring, power supply voltages, and the output from a tilt sensor used for automatically referring the elevation angle to local zenith [*Janssen,* 1985]. The uncertainty on the count measurements is estimated by discarding the first raw data package (to ensure all transients and pointing movements have ceased), averaging the remaining four measurements, and calculating the standard deviation for the four measurements. The thermistor voltages monitoring the hot and reference loads, the IF/mixer, and the noise diode are converted to temperatures via previously determined calibration coefficients.

The water vapor spectral line at 22.235 Ghz is rather weak, which implies that radiation emitted by water vapor molecules at high altitudes will be only slightly attenuated when it arrives at the surface of the Earth, for all realistic densities of atmospheric water vapor. A complication is that liquid water also emits radiation of comparable or greater intensities than the vapor at these frequencies (22 GHz). However, the two radiation processes exhibit distinctly different spectral features [e.g. *Becker and Autler,* 1946; *Van Vleck,* 1947; *Goldstein,* 1951], and the liquid contribution can be separated from the vapor contribution by measuring the emission at two different frequencies. Although the instrument takes measurements at three frequencies (20.7, 22.2, and 31.4 GHz), only measurements at two frequencies (20.7 and 31.4 GHz) are actually used in the calculation of the integrated precipitable water vapor with the higher frequency contributing most to the estimate of the liquid water component. The choice of frequencies has been discussed by numerous authors [e.g., *Westwater,* 1967, 1978; *Resch,* 1983; *Gary et al.*, 1985]. *Gary et al.* [1985] found that the addition of measurements from the third frequency channel at 22.2 GHz may produce a slight (<7%) improvement in the rms performance over the two-frequency approach. The lower frequency used in the calculation of the precipitable water vapor (20.7 GHz) is positioned close to the center of the water vapor emission line, while the other frequency (31.4 GHz) is placed well away from the line center. Measurements at this frequency (20.7 GHz) are better correlated with the integrated water vapor than are measurements at the line center [*Westwater,* 1967].

Calibration

The basic calibration method for the radiometer is the "tip curve" or elevation scan method with each channel being treated independently [*Resch,* 1983; *Hogg et al.,* 1983]. Tip curves are obtained by measuring the sky brightness as a function of elevation angle (air mass). Seven sky measurements between elevations of 20° and 160° spaced in equal air mass intervals constitute the data for a tip curve. A second, orthogonal, scan follows the first scan. The data from these orthogonal tip curves were used to solve for the system gain (G^T_{sys}) and zenith opacity (τ_z) for each channel by performing a least squares solution to the equation

$$N_{ant} = N_{ref} + G^T_{sys}\,[T_{atm} - T_{ref} + (T_c - T_{atm})e^{-\tau_z m}] \qquad (1)$$

where N_{ant} and N_{ref} are antenna and reference load counts; T_{atm} is the effective radiating temperature of the atmosphere, T_{ref} is the reference load temperature, and T_c the extraterrestrial background temperature; m is the air mass; and τ_z is the zenith opacity. A spherically symmetric model with a 3-km scale height is assumed as the measurement model for the wet troposphere. This condition is approximately satisfied during periods of good, cloudless weather. If clouds are present, or if the atmosphere is unsettled, or it is raining, then this approximation fails. The tip curve method is sensitive to any inhomogeneities in the atmosphere, but provided that tip curves are carried out at different azimuthal angles (generally two orthogonal azimuths), these inhomogeneities can be detected. If the atmosphere is very inhomogeneous (for example, when significant quantities of liquid water are present in cloudy weather), these data are downweighted in the calibration procedure.

The gain calibration is maintained between good quality tip

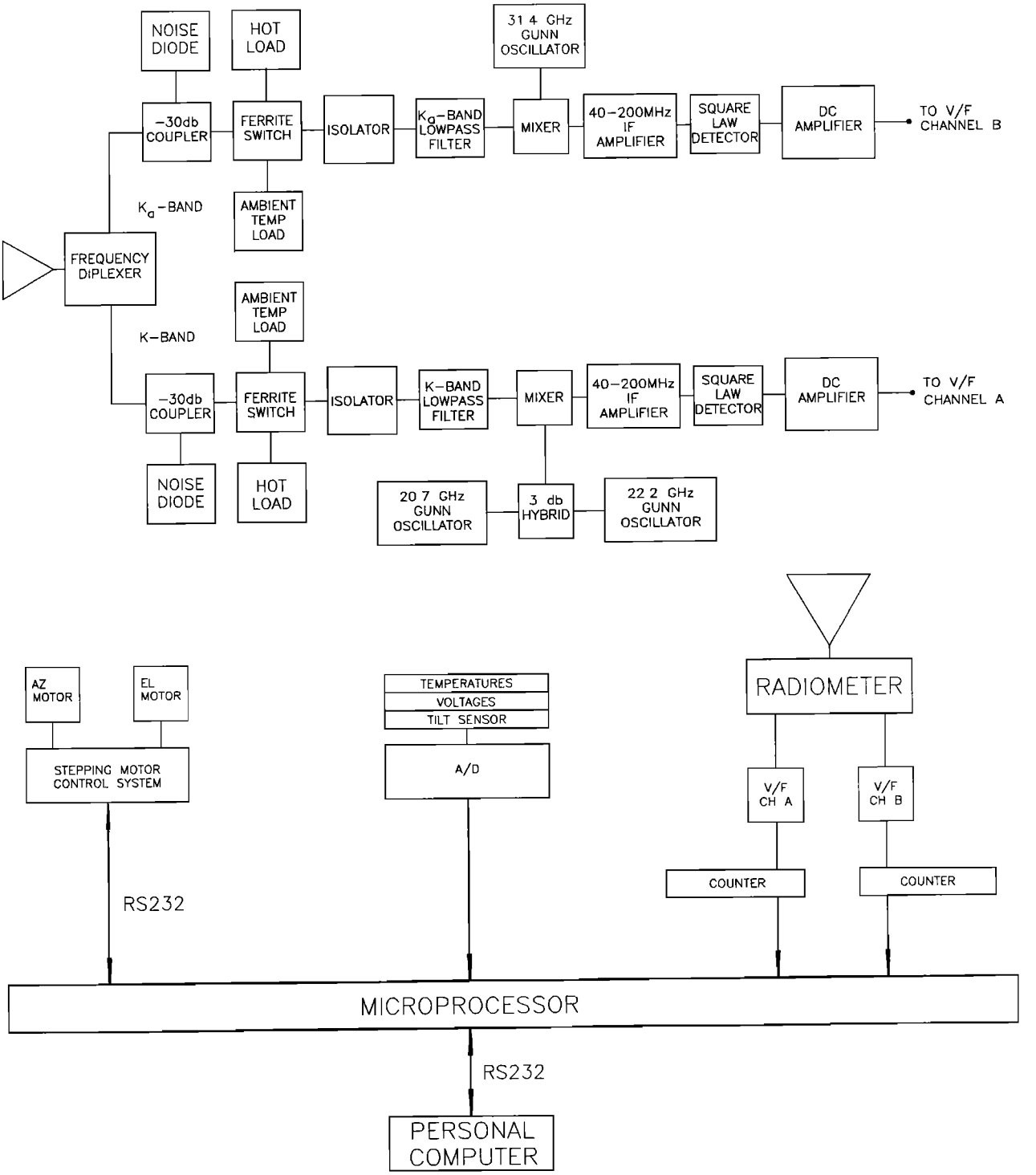

Fig. 1. (*a*) Microwave circuit and (*b*) block diagram of the J-series microwave water vapor radiometer J03.

curves and during periods of inclement weather by calculating an instrument gain

$$G_{ins} = \frac{[N_{hot} - N_{ref}]}{[T_{hot} - T_{ref}]} \tag{2}$$

and forming a gain ratio

$$R = \frac{G_{sys}^{T}}{G_{ins}} \tag{3}$$

by using the system gain calculated from high quality tip curves. The instrument gain is calculated using the hot and reference loads as waveguide terminators. The hot load is maintained at a temperature of 376 ± 0.02 K. The reference load is inside the radiometer enclosure, which is temperature regulated at about 310 ± 2 K. The reference load tracks the diurnal temperature variation but with greatly reduced amplitude.

The calibration scheme must accurately reproduce the tip calibration during times when the tip calibration is valid and must be stable enough to maintain calibration through several hours of inclement weather. A running average gain ratio ($<R>$) as well

as a running average instrument gain ($<G_{ins}>$) is maintained to reduce the random uncertainty. The average instrument gain is updated using a weighting factor, f, as follows:

$$\langle G_{ins}\rangle = (1-f)\langle G_{ins}\rangle_{old} + fG_{ins} \quad (4)$$

where G_{ins} is the instantaneous instrument gain value and $<G_{ins}>$ is the un-updated average instrument gain. A shortcoming of this averaging is that the average value tends to lag behind the instantaneous value. As f increases, the discrepancy between the instantaneous and averaged values, Δ, decreases, but the uncertainty in the instrument gain increases.

The average gain ratio is updated using a different weighting factor, g:

$$\langle R\rangle = (1-g)\langle R\rangle_{old} + gR. \quad (5)$$

Since the gain ratio is much more stable than the instrument gain, the averaging constant (g) can be much less than the constant for the instrument gain (f).

To maintain the calibration requirement of

$$\frac{\Delta}{\langle R\rangle} < 0.001, \quad (6)$$

the weighting factors (f and g) are chosen such that the difference (Δ) between the instantaneous and averaged values is less than the noise [*Gipson and Lundqvist*, 1986]. Using weighting factors of $f=0.1$ and $g=0.01$ contributes 0.3% to the systematic error. This amounts to 0.4 mm of precipitable water vapor.

The line-of-sight brightness temperatures are given by

$$T_{br} = T_{ref} + \frac{N_{sky} - N_{ref}}{\langle G_{sys}\rangle}, \quad (7)$$

where N_{sky} are the counts measured by the radiometer when looking at the sky, N_{ref} are the counts when the reference load is the waveguide terminator, T_{ref} is the physical temperature of the reference load waveguide terminator, and $<G_{sys}>$ is the system gain defined as

$$\langle G_{sys}\rangle = \langle R\rangle \times \langle G_{ins}\rangle. \quad (8)$$

These brightness temperatures are converted into line-of-sight opacities for use in the retrieval algorithm to obtain the "wet" component of the extra signal delay due to the troposphere and the integrated precipitable water vapor content of that column of the atmosphere.

Precipitable Water

By using various approximations, several algorithms can be developed to estimate the "wet" delay and the water vapor content of the particular column of atmosphere being observed from the WVR brightness temperatures [e.g., *Resch*, 1983; *Gary et al.*, 1985; *Johansson et al.*, 1987; *Robinson*, 1988]. The model that yields the path delay from the WVR measurements is called the retrieval algorithm. The retrieval algorithm used in this study was developed by Gary et al. [1985] and *Gary and Keihm* [1986, private communication, 1989]. The retrieval algorithm uses an archive of atmospheric (radiosonde) profiles to calculate path delays and all observables for a site. These are then used to calculate the "average" properties and the departures from average for each radiosonde. The retrieval coefficients are computed by a least squares minimization technique involving the covariance matrices of the observable and path delay departures from their averages (see *Westwater* [1972] for details of the statistical procedure). The retrieval algorithm uses opacities (τ_i) calculated from the brightness temperatures measured by the WVR.

The calculation of these opacities from the brightness temperatures uses an "effective temperature" (T_{eff}) for the atmospheric emission [*Resch et al.*, 1985]. The site and seasonal variation in T_{eff} of 4.5 K [*Resch*, 1983; *Resch et al.*, 1985] contributes about 0.5 mm to the systematic error in the integrated water vapor measurement, although this bias error will change from night to night.

The path delay due to water vapor (PD_{wet}), when expressed as a departure from the long-term site average and when the observables are also expressed as departures from their long-term site averages, is empirically related to these various observables by [*Gary et al.*, 1985]

$$PD_{wet} - \langle PD_{wet}\rangle = \sum_{i=1}^{4} C_i(O_i - \langle O_i\rangle), \quad (9)$$

where $<PD_{wet}>$ is the site specific average path delay and C_i are site specific retrieval coefficients. The observables O_1 and O_2 are the opacities at 20.7 and 31.4 GHz, respectively, O_3 is the surface temperature in Kelvin, and O_4 is the surface pressure in millibars. The averaged quantities are the corresponding site specific averages for these observables. Either of two sets of averages ($<O_i>$) and retrieval coefficients (C_i) may be used to determine the path delay depending upon the weather conditions. One set is valid for "clear" conditions and the other is valid for "cloudy" conditions. *Gary and Keihm* [1986, private communication, 1989] suggest using a liquid burden criterion for determining the set of coefficients to be used. If the liquid burden is less than 100 μm of precipitable water, "clear" coefficients should be used.

The integrated precipitable water vapor content (PW in centimeters of precipitable water) of the particular column of atmosphere being observed is empirically related to the wet path delay by [*Resch*, 1983]

$$PW = \frac{PD_{wet}}{[5.6 - 0.022(T - 308)]} \quad (10)$$

where PD_{wet} is expressed in centimeters of path delay and T the surface temperature in Kelvin.

Data and Error Analysis

The observation sequence for the WVR measurements consisted of two orthogonal tip curves interspersed with zenith line-of-sight (LOS) measurements. After the second tip curve and zenith LOS measurement, azimuth scans were done at elevations of 30° and, occasionally, 45°. Because the lidar exclusively samples at the zenith, only the WVR zenith measurements were considered in this study, and consequently, the WVR data set is not as dense as the lidar data set. The observing sequence was repeated at intervals of about 33 min. Because each tip curve produces an estimate of the zenith opacity (and hence the zenith brightness temperature) for each frequency, the data consist of clumps of four data points (two tip and two LOS points spread over a time range of about 3.5 min) separated by approximately 33 min. The WVR data were processed to produce clumps of four (two tip and two LOS) measurements of the integrated precipitable water vapor and their associated uncertainties. Each set of four measurements was averaged to produce a vapor measurement approximately every 33 min. WVR data taken simultaneously with the lidar exist for three nights during the experiment period (April 11-12, April 16-17, and April 17-18, 1989). The choice of "clear" or "cloudy" retrieval coefficients and averages was determined by examining the lidar results for cloud base height and by visual examination of the prevailing meteorological conditions. If the lidar results showed significant cloud cover in the zenith direction (as indicated

by no usable lidar data above a few kilometers), then "cloudy" conditions were deemed to exist (April 17-18) and the coefficients and averages were chosen accordingly. *Gary and Keihm* [1986, private communication, 1989] suggest using a liquid burden criterion for determining the set of coefficients to be used. If the liquid burden is less than 100μm of precipitable water, "clear" coefficients should be used. However, because the radiosonde data used in the derivation of the retrieval coefficients do not provide any direct indication of the presence of liquid water, the regression analysis for the liquid water retrieval relies upon a model for the distribution of liquid (clouds) derived from the radiosonde relative humidity measurements. Due to problems with the liquid water retrieval coefficients, the liquid burden criterion for choosing coefficients was not used. As a check on the error introduced by using incorrect coefficients, data from the period determined to be "cloudy" from the lidar results (April 17-18) were processed, using both "clear" and "cloudy" sets of coefficients. The mean difference between the two determinations of the precipitable water vapor content ("cloudy" minus "clear") was 0.2 mm of precipitable water vapor.

The final uncertainty in the radiometric water vapor estimates is composed of errors from a variety of sources: the "known" uncertainties in the measurements of the WVR antenna temperatures (brightness temperatures) and the emission model uncertainty. The brightness temperature uncertainties were calculated by propagating the "known" uncertainties through the reduction procedure and then including (in quadrature) the emission model uncertainty in the final result. The known uncertainties are the uncertainties in the count measurements for sky, reference load, and hot load measurements that are recorded in the field data log. These can be compared with their characteristic values as a quality control check. Characteristic standard errors for these parameters were calculated from the long term behavior of the parameters. These characteristic uncertainties (σ) are tabulated in Table 1 for both count parameters and physical temperature parameters. Also listed in Table 1 are the contributions to the uncertainties on the brightness temperatures (using equation (7)). The logged uncertainties for the count measurements are typically about 4 - 10 counts (0.1 - 0.3 K uncertainty in the brightness temperature), which compare well with the characteristic values in Table 1. Characteristic uncertainties for the physical temperature measurements are $\pm$ 0.02 K for the hot load and $\pm$ 0.18 K for the reference load measurements.

Propagating these uncertainties through the analysis gives the random uncertainties on the gains and the brightness temperatures.

TABLE 1. Characteristics: WVR J03

	Channel	σ	$\delta\sigma(T^{bs})$, K
Hot load	1,2	0.019 K	0.08
	3	0.011 K	0.05
Reference load	1,2	0.18 K	0.18
	3	0.17 K	0.17
Hot counts	1,2	6 cts	0.09
	3	6 cts	0.09
Reference counts	1,2	5 cts	0.20
	3	5 cts	0.20
Sky counts		4-10 cts	0.2-0.4

The random gain uncertainties contribute approximately 0.06 K to the uncertainties on the brightness temperatures. During periods of good weather the brightness temperature random uncertainties are typically less than 0.5 K (see Figure 2 for an example from April 17, 1989).

The emission model uncertainty is an estimate of the uncertainty introduced by the retrieval algorithm used in getting integrated water vapor (via various emission models) from the brightness temperature measurements at the two frequencies used in this study. Even though this is poorly understood, it is the best estimate available for the uncertainty on the vapor measurements. This uncertainty is calculated following the precepts of *Gary and Keihm* [1986, unpublished manuscript, 1989], who recommend that the total uncertainty consist of a performance expectation and an emission model uncertainty. The performance expectation of the algorithm takes into account the random uncertainty in the brightness temperature measurement and is equivalent to the "known" uncertainties defined above. The emission model uncertainty attempts to correct for the uncertainties in the emission models of *Rosenkranz* [1988] (for oxygen) and *Liebe and Layton* [1987] (for vapor). In calculating the performance expectation the *Gary and Keihm* [1986, private communication, 1989] retrieval algorithm uses a brightness temperature random uncertainty of 0.5 K. Because the brightness temperature random uncertainties for this experiment are slightly less than 0.5 K, the performance expectations quoted by B. L. Gary and S. J. Keihm (private communication, 1989) were used in the error analysis, giving a slight overestimate of the actual integrated water vapor random uncertainty.

Gary and Keihm [1986] suggest a total emission model uncertainty of about 8% of the retrieved parameter. This contributes from 0.4 mm (April 11-12) to 1.7 mm (April 17-18) to the systematic uncertainty in the integrated water vapor results. However, recent estimates for the actual uncertainties in the emission models have been made by *Davis et al.* [1985] and *Elgered et al.* [1991]. *Elgered et al.* [1991] estimate that the uncertainty for the water vapor emission model is about 6% (0.3 mm of precipitable water vapor for April 11-12, 0.6 mm for April 16-17, and 1.2 mm for April 17-18). The uncertainty for the oxygen emission model is estimated to be less than 0.4 mm of precipitable vapor. *Elgered et al.* [1991] also note that if the size of the liquid drops becomes comparable to the wavelength of the radiation, the algorithm over estimates the vapor. However, experience has shown that in these cases (rain) the WVR is ineffective for calculating the water vapor. In fact, any moisture (such as dew or rain) on the mirror flat or the Teflon window covering the microwave horn completely invalidates the WVR data.

The total uncertainties for the individual WVR precipitable water vapor measurements (Table 2) range from 0.9 mm for cloud-free conditions (April 11-12) to 1.9 mm for cloudy conditions (April 17-18). These uncertainties can be separated into random and bias errors. Contributions to the bias errors come from systematic errors in the effective temperature and gain calibrations and from the emission model uncertainties. These contributions are tabulated in Table 2. The corresponding random errors range from 0.4 mm to 1.3 mm.

3. Raman LIDAR Moisture Measurements

Lidar System

The lidar system used in the investigation has been described by *Melfi and Whiteman* [1985] and *Melfi et al.* [1989]. *Whiteman et*

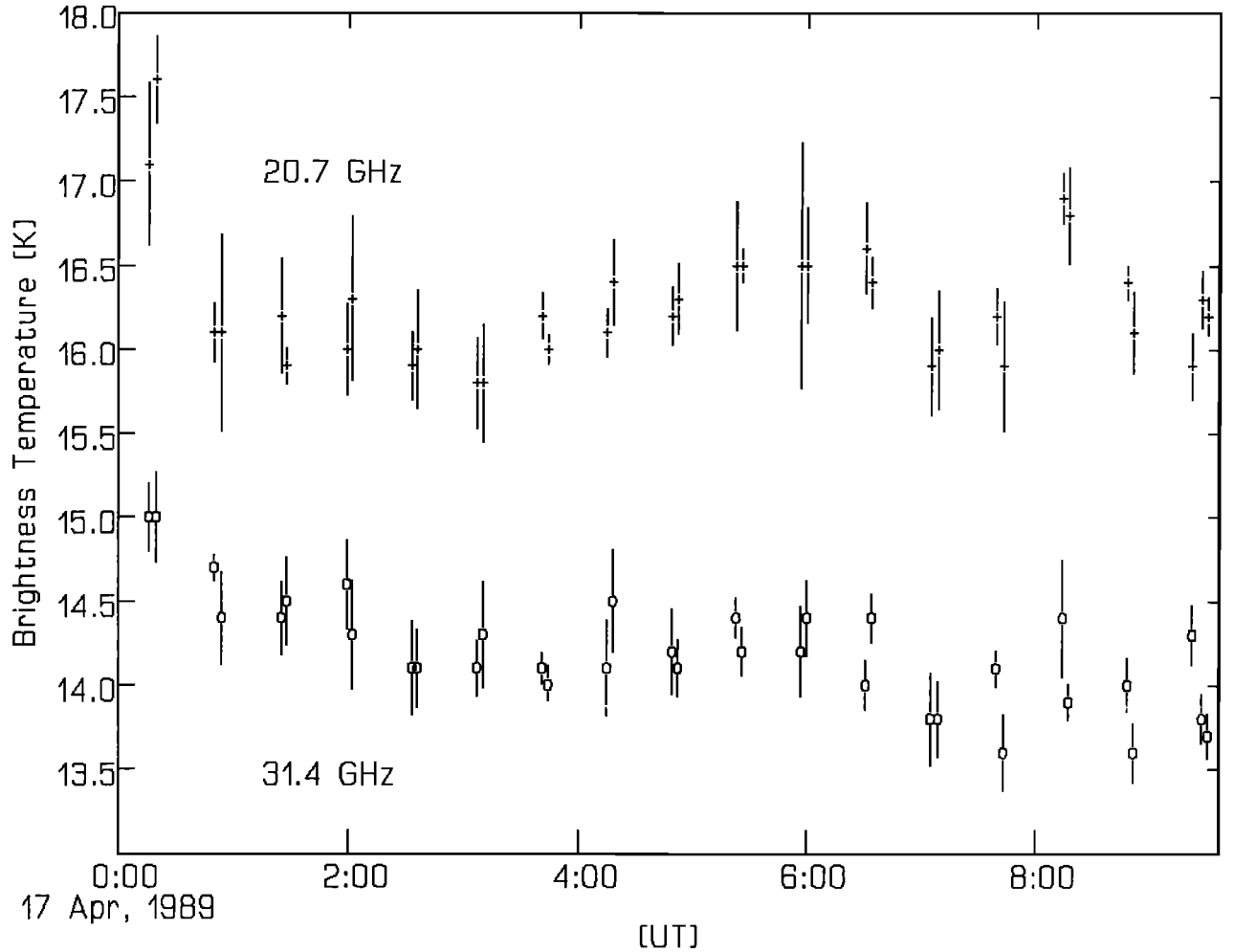

Fig. 2. Zenith sky brightness temperatures at 20.7 and 31.4 GHz measured by the WVR at Wallops Island, Virginia, for April 17, 1989. The error bars represent the random uncertainties on the measurements.

al. [1991] give a more complete description of the system and measurement procedures that were used during the ATMIS experiment.

A block diagram of the lidar instrument is given in Figure 3. The lidar consists of a Nd:YAG laser operating at the tripled wavelength of 355 nm. A 0.75-m diameter Dall-Kirkham telescope collects the scattered laser light (as the laser pulse propagates through the atmosphere), which beam splitters divide into three channels: one sensitive to Raman scattering by water vapor molecules at 408 nm, a second sensitive to Raman scattering by nitrogen at 387 nm, and the third sensitive to scattering by molecules and aerosols at the laser wavelength (355 nm). Interference filters select these Raman wavelengths. Photomultiplier tubes (PMTs) detect the backscattered radiation in each of the three channels and provide output signals to both A/D converters and photon counters (PCs). The A/D data are smoothed from their maximum altitude resolution of 30 m (200 ns) to a resolution of approximately 100 m using a "nearly equal ripple" low-pass filter [*Kaiser and Reed*, 1977]. The Pcs provide an altitude resolution of 150 m. From near the surface to an altitude of approximately 2 km, A/D data are generally used, with PC data being used above this altitude. The PC data tend to be of higher quality but cannot be used below 2 km because the high atmospheric backscatter intensity from short ranges leads to PC saturation. Signals from approximately 1000 laser shots are collected, after which the accumulated signals acquired by the A/Ds and PCs are stored on magnetic disk. The sum of the squares of the A/D data are also stored in order to compute the standard error of the A/D data. The standard errors for the PC data are estimated assuming Poisson statistics (i.e., the noise equals the square root of the total number of events).

TABLE 2. WVR Integrated Water Vapor Measurements in Millimeters

Date	Uncertainties		
	April 11-12	April 16-17	April 17-18
Total precipitable vapor (WVR)	5	10	21
Random error	0.4	0.4	1.3
Systemaic error			
Emission model (WV)[a]	0.3	0.6	1.2
Emission model (O_2)[a]	0.4	0.4	0.4
Gain calibration	0.4	0.4	0.4
T_{ef} calibration	0.5	0.5	0.5
Total systematic	0.8	0.9	1.4
Total error (WVR)	0.9	1.0	1.9

[a] From *Elgered et al.* [1991]

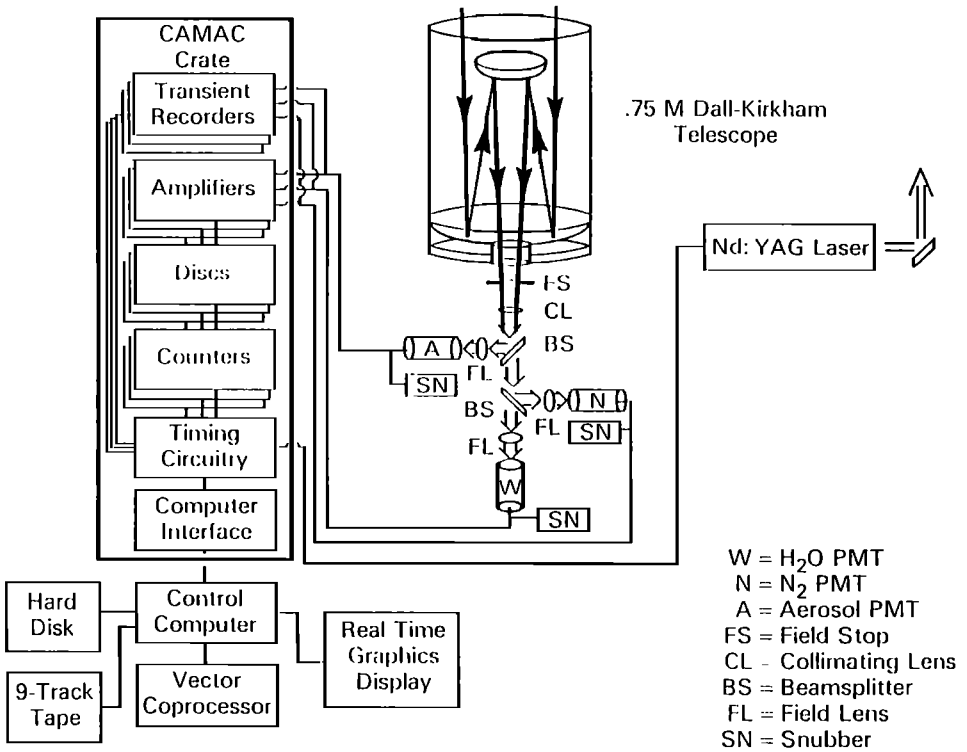

Fig. 3. Block diagram of the water vapor Raman lidar system. "Discs" refers to the discriminators.

Theory

As shown by *Melfi* [1972], the ratio of Raman scattering by water vapor in the atmosphere to that by nitrogen is proportional to the value of the atmospheric water vapor mixing ratio. The water vapor mixing ratio is the mass of water vapor divided by the mass of dry air in a given volume. A small correction to the calculated ratio is made which takes into account differential atmospheric attenuation at the two Raman wavelengths. Under clear atmospheric conditions this correction is less than 5% at an altitude of 7 km and is smaller at lower altitudes. The actual amount of this attenuation correction is estimated from data acquired from the lidar aerosol channel, which records the signal backscattered at the laser wavelength (355 nm).

Scattering due to atmospheric aerosols can be analyzed in an analogous manner to that for water vapor. The lidar aerosol channel data are sensitive to scattering by molecules and Mie scattering by aerosols. Since Mie scattering increases abruptly when the laser beam encounters a cloud, the cloud base height is easily determined from the aerosol scattering ratio profile. However, because of this greatly enhanced Mie scattering, clouds rapidly attenuate the laser light, so that the water vapor retrieval is confined to altitudes below cloud base.

Calibration

The water vapor mixing ratio is proportional to the ratio of Raman scattering by water vapor to Raman scattering by nitrogen. The calibration constant relating the measured lidar ratio to the water vapor mixing ratio is determined by computing a weighted least squares regression of the lidar ratios to the water vapor mixing ratios obtained from coincident radiosonde measurements. This regression yields a single calibration constant relating the lidar ratios to the water vapor mixing ratios. The lidar ratios were calibrated using the radiosondes launched at Wallops Island during the ATMIS experiment. Three or four balloons, each carrying three separate radiosonde sensor packages, were launched each night in order to compare the temperature- and humidity-sensing elements of each package. The PC data were calibrated with the radiosonde packages, since the PC data generally have a higher signal/noise ratio than the A/D data. Since the A/D and PC data both include the altitudes between 2 and 6 km, the A/D data were then calibrated using the PC calibration as well as the radiosonde comparisons. Each balloon took about 20 min to ascend to 6 km; therefore the lidar PC data were averaged over this 20-min period to reduce the random error in the lidar data. (Since there was little change in the meteorological conditions during the course, the uncertainty introduced by this 20-min averaging was insignificant.) Radiosonde mixing ratios corresponding to relative humidities less than 20% were not used in the lidar calibration, because two of the three radiosonde packages have previously not provided reliable moisture measurements below this value [*Melfi et al.*, 1989; *Wade and Wolfe*, 1989]. A procedure designed to compensate for any small changes in channel sensitivity was used to maintain a constant system calibration during the ATMIS experiment [*Whiteman et al.*, 1991].

During the seven nights the lidar was operating there were 43 individual comparisons between the lidar and radiosonde mixing ratios; these comparisons were obtained from 15 radiosonde launches (on two of the launches one of the sensor packages failed). Over the first five nights, which included 10 balloons with 29 radiosonde comparisons, the standard deviation of the mean of the lidar calibration constant was slightly greater than 1%. Thus the lidar was able to maintain a single calibration value with excellent stability. After the fifth night some minor changes to the transmitter optics and electronics necessitated recalibrating the lidar data. During the last two nights the standard deviation of the mean of the lidar calibration constant was approximately 3% from 5 balloons with 14 radiosonde intercomparisons.

A comparison between the lidar mixing ratios derived with the

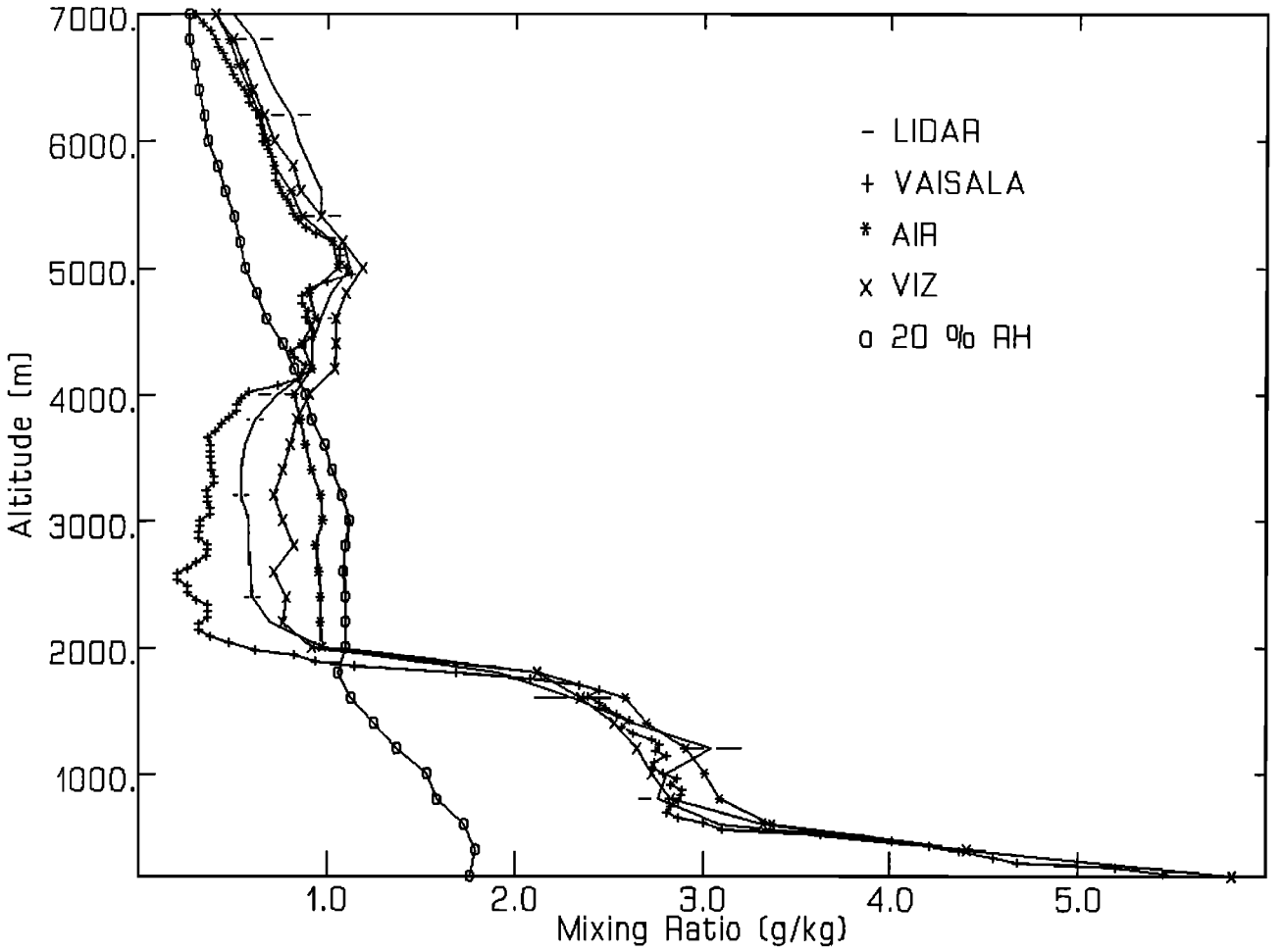

Fig. 4. Water vapor mixing ratio profiles measured using the lidar system and the VAISALA, AIR, and VIZ radiosonde packages on a balloon launched on April 17, 1989, at 0455 UT at Wallops Island, Virginia. For comparison, mixing ratios corresponding to a constant 20% relative humidity are also shown. The symbols only identify the different radiosonde profiles and do not represent the actual measurements. Representative error bars are shown for the lidar profile.

constant system calibration and the mixing ratios measured by the various radiosonde sensors is shown in Figure 4. The data in the figure were acquired during the early hours of April 17, 1989. The balloon was launched at 0455 UT, and the lidar data were acquired over a 20-min period after the balloon launch. The data in Figure 4 indicate that from the surface to about 2 km and again from 4 km to 7 km all four moisture measurements agree to approximately ± 5%. Note the error bars on the lidar data indicate a standard error of about ± 5% below 2 km and about ± 0.1 g/kg above 4 km. Mixing ratios corresponding to a constant 20% relative humidity are also shown. The disagreement among the sensors for altitudes between 2 and 4 km is due to the different radiosonde sensors and calibration procedures. In this altitude region the VIZ and AIR sensors both indicate a mixing ratio of about 1 g/kg, which is slightly less than a mixing ratio corresponding to 20% relative humidity. Both of these sondes use carbon hygristors with similar calibration procedures which limit sensitivity for relative humidities less than 20% [*Brousaides*, 1975]. The VAISALA sensor uses a capacitive device with a different calibration procedure which apparently maintains sensitivity even for very dry atmospheric conditions, as shown in Figure 4. The lidar, on the other hand, indicates an intermediate level of moisture in this altitude region.

Precipitable Water

Before computing the integrated water vapor content, the A/D and PC calibrated mixing ratio profiles were merged to give a single profile extending from about 100 m to approximately 6.75 km or cloud base (if the cloud base was lower than 6.75 km). For a 2-min average this top altitude was chosen, since it corresponds to about 10% random error in the lidar data. The altitude where the A/D and PC data profiles were merged is chosen at the lowest altitude where the PC data are not saturated; this generally occurs between 1.5 and 2.0 km. Thus the A/D data were used from about 100 m to this transition altitude, while the PC data were used above the transition altitude.

Precipitable water, PW (in millimeters), is computed using the following equation [*Haltiner and Martin*, 1957]:

$$PW = \frac{-0.1}{g} \int_{P_0}^{P_1} \frac{w(P')}{1000 + w(P')} dP', \qquad (11)$$

where g is the acceleration due to gravity, P is the pressure (in millibars), and $w(P)$ is the water vapor mixing ratio (in grams per kilogram). Since the mixing ratios derived from the lidar data were computed as a function of altitude rather than pressure, the radiosonde pressures were logarithmically interpolated to the lidar

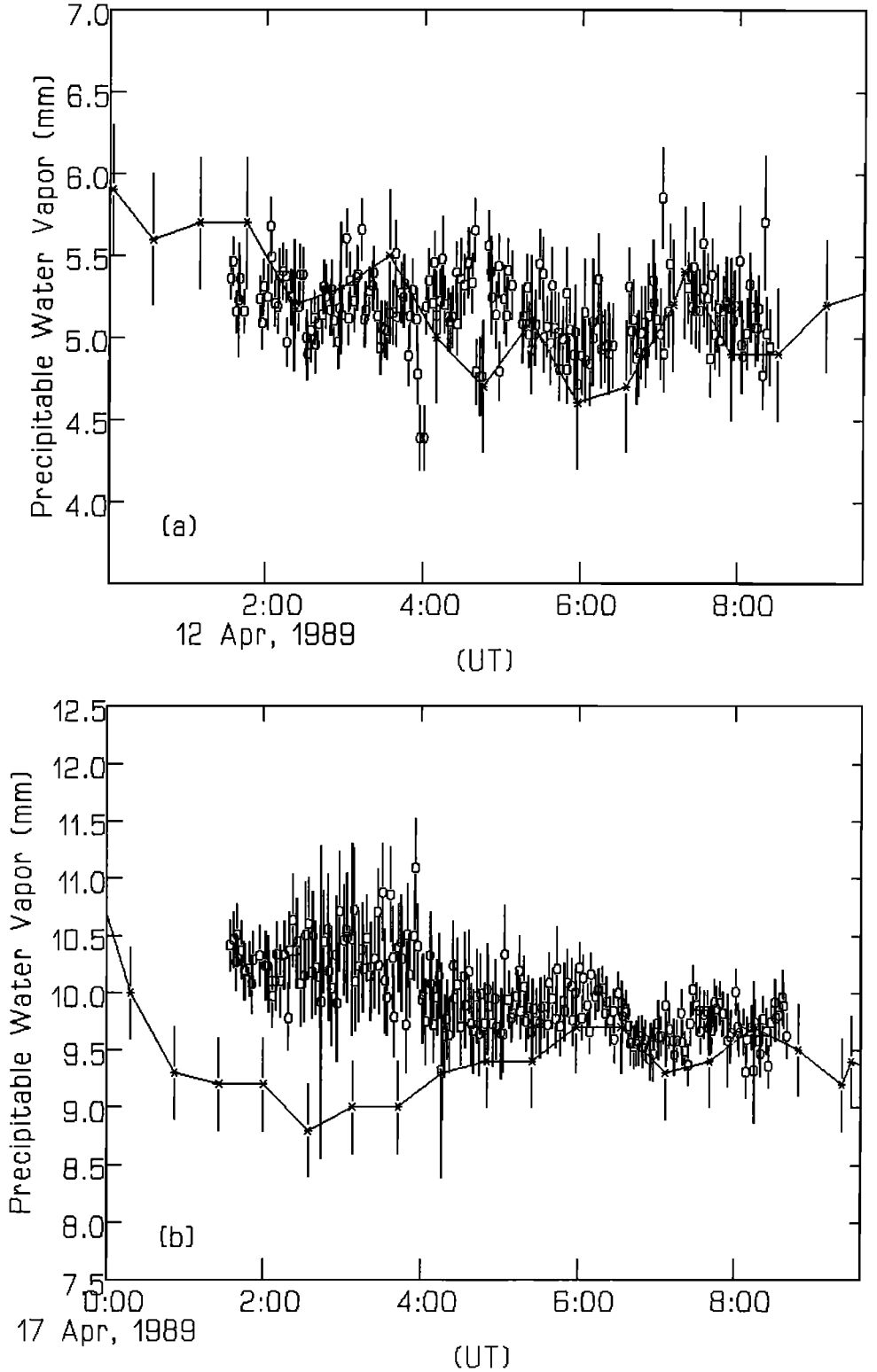

Fig. 5. Integrated precipitable water vapor (in millimeters) from lidar (circles) and WVR (stars) measurements at Wallops Island, Virginia, for (*a*) April 11-12, 1989, (*b*) April 16-17, 1989, and (*c*) April 17-18, 1989. The WVR measurements are connected by the line. The error bars represent the random uncertainty on the measurements.

altitudes before using this equation. The altitude increment used for the lidar data is 150 m which corresponds to the spacing of the PC data. Since the altitude of the lowest lidar-derived mixing ratio value is about 100 m, the surface mixing ratio was interpolated in time from the radiosonde data. Precipitable water estimates were computed from 30-min average lidar mixing ratio profiles as well as the 2-min average profiles in order to directly compare with the precipitable water values obtained from the microwave radiometer (WVR) measurements. The lidar-derived precipitable water values were computed by using equation (11)

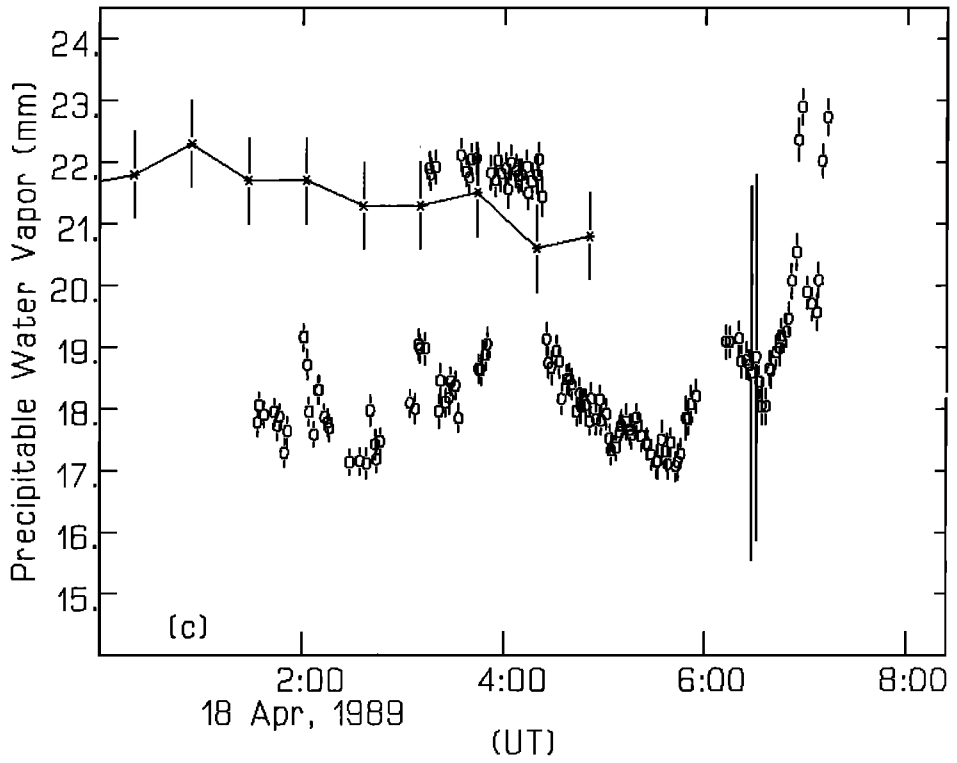

Fig. 5. (continued)

between the surface and 6.75 km. Since a small amount of water vapor exists above this altitude, the lidar measurements of precipitable water will be biased slightly smaller than the true amounts. This error will be discussed in the next section.

Errors

There are various sources of error which affect the precision of the lidar-derived water vapor mixing ratio measurements. The first source of error is due to the random error associated with the

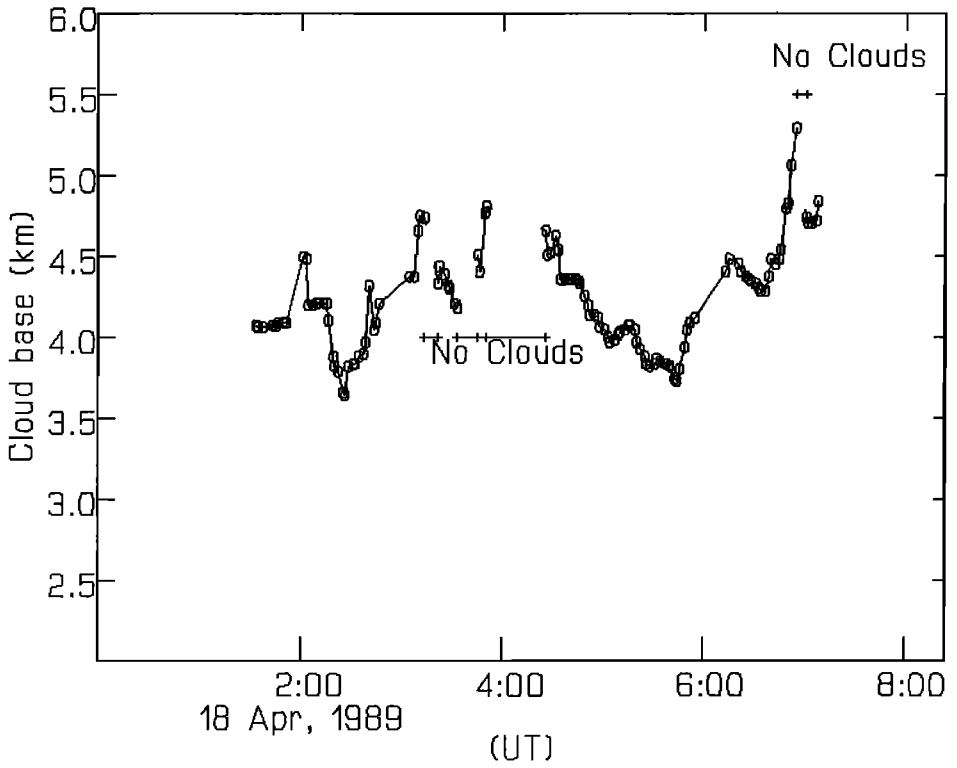

Fig. 6. Cloud base height at Wallops Island, Virginia, for the night of April 17-18, 1989, inferred from the lidar measurements. Cloud free periods are indicated by gaps in the line.

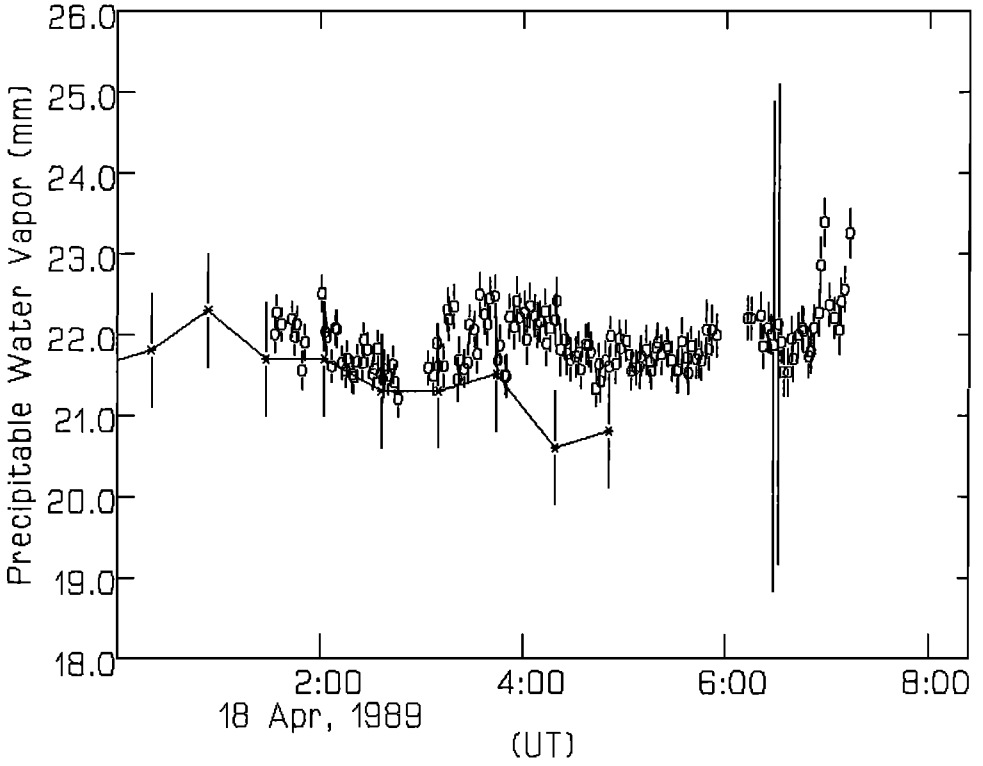

Fig. 7. Integrated precipitable water vapor measurements (in millimeters) at Wallops Island, Virginia, for April 17-18, 1989. The lidar measurements (circles) have been augmented by measurements from VAISALA radiosondes launched every three hours. The WVR measurements (stars) are connected by the line. Error bars represent the random uncertainty on the measurements.

lidar data; both Raman water vapor and nitrogen channels contribute to this error. Since the signal-to-noise-ratio of the lidar data decreases with altitude, this error increases with altitude. For a 2-min average profile the random error is slightly less than 10% at an altitude of 6.75 km. Averaging the data reduces the random error, so that for a 30-min average this random error becomes about 1-2%.

A second error source is the uncertainty in the calibration constant relating the lidar Raman water vapor to nitrogen ratio to the water vapor mixing ratio. Since this calibration constant is derived from the radiosonde comparisons, this constant will depend on the accuracy of the balloon measurements.

Unfortunately, there are very limited data with which to assess the accuracy of the radiosonde humidity measurements. Manufacturer's specifications list ± 4% for the carbon hygristor humidity sensors used by the VIZ and AIR packages [viz specifications, 1987] and ± 2% for the VAISALA capacitive sensor [VAISALA specifications, 1986]. Laboratory measurements have obtained slightly higher values. *Brousaides* [1975] found mean errors for the carbon hygristor to vary from 0% to ± 8% depending upon temperature. A National Bureau of Standards test (1981) found a systematic error of 4-5% in the VAISALA measurements of relative humidity. However, since these tests are several years old and since the errors have shown some dependence on the particular manufactured lot, it is not clear whether or not these results would apply to the sensors flown during ATMIS.

The lidar calibration constant was obtained from the entire ATMIS radiosonde data set, which is composed of humidity measurements obtained from both types of humidity sensors, two carbon hygristor sensors and one capacitive sensor. The impact of errors in the calibration of the sensors on the lidar measurements is thus reduced by averaging over the data set. For the ATMIS procedure described above, the average of the lidar calibration constants varied by 1-3% over the course of the experiment.

A third source of uncertainty is associated with the differential transmission correction which is applied to the lidar ratios. Since the differential transmission due to Rayleigh scattering can be computed with high accuracy, differential scattering due to Mie scattering from aerosols accounts for this uncertainty. This differential aerosol transmission is estimated from the aerosol scattering ratio obtained from the lidar data. During the ATMIS experiment the aerosol loading was generally small, so that the corresponding error in this differential transmission is much smaller than the random and calibration errors discussed above.

The lidar underestimates the precipitable water, since in clear conditions the lidar mixing ratio measurements are integrated from the surface to 6.75 km. This bias in the lidar measurements was estimated by computing the precipitable water, using "hybrid" profiles which were constructed by using the lidar mixing ratio values from the surface to 6.75 km and the radiosonde values from 6.75 km to an altitude of nearly 16 km (100 mbar). These computations were performed using each of the three radiosonde sensor packages. For the nights of April 11-12 and April 16-17 when the skies were cloud free, the precipitable water measurements which used only the lidar data were approximately 3-4% lower than those which used the "hybrid" profiles. This bias appears regardless of radiosonde sensor type used to construct the "hybrid" profiles. When clouds were present such that the maximum altitude for the lidar data is lower than 6.75 km, this bias naturally increases. During the night of April 17-18 the lidar acquired data while scattered clouds drifted over the ATMIS site.

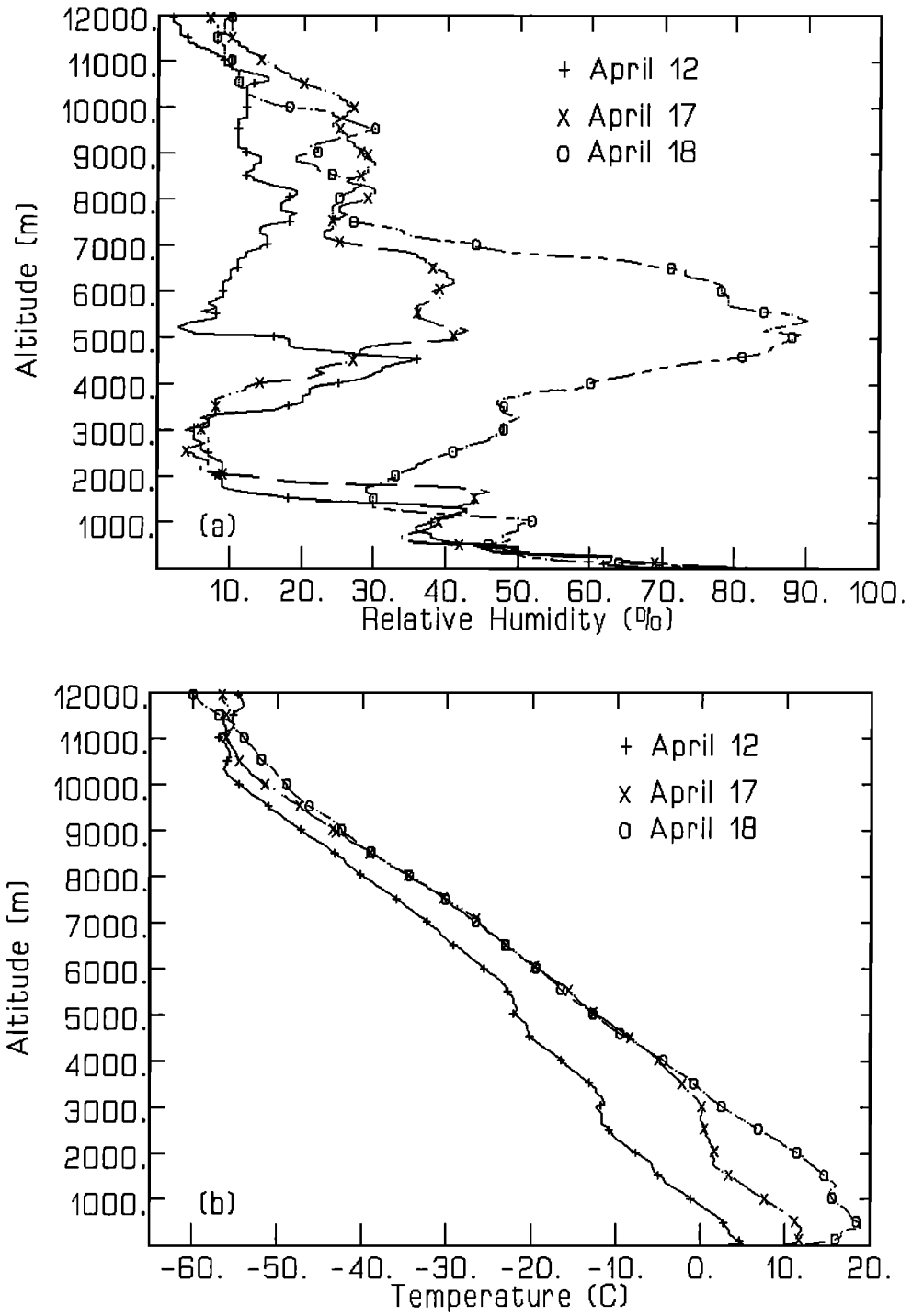

Fig. 8. (*a*) Relative humidity and (*b*) temperature profiles measured with the VAISALA radiosonde package at Wallops Island, Virginia. The radiosondes were launched at 0500 UT on April 12, 1989 (pluses), 0455 UT on April 17, 1989 (crosses), and 0457 UT on April 18, 1989 (circles).

The lidar data indicated that the cloud base was approximately 4 km. The precipitable water, computed to cloud base from the lidar data only, was approximately 25% lower than that computed using the "hybrid" lidar plus radiosonde profiles. However, during those intermittent times when clouds were not overhead such that the lidar data could be used to 6.75 km, this error decreased to the clear condition value of approximately 3%.

4. Results

The integrated precipitable water vapor measurements from the lidar and the WVR for the three nights of the experiment are shown in Figures 5*a*-5*c*. Although the lidar and the WVR operated faultlessly for 7 nights, due to problems with the post data acquisition archiving procedures for the WVR, data from a

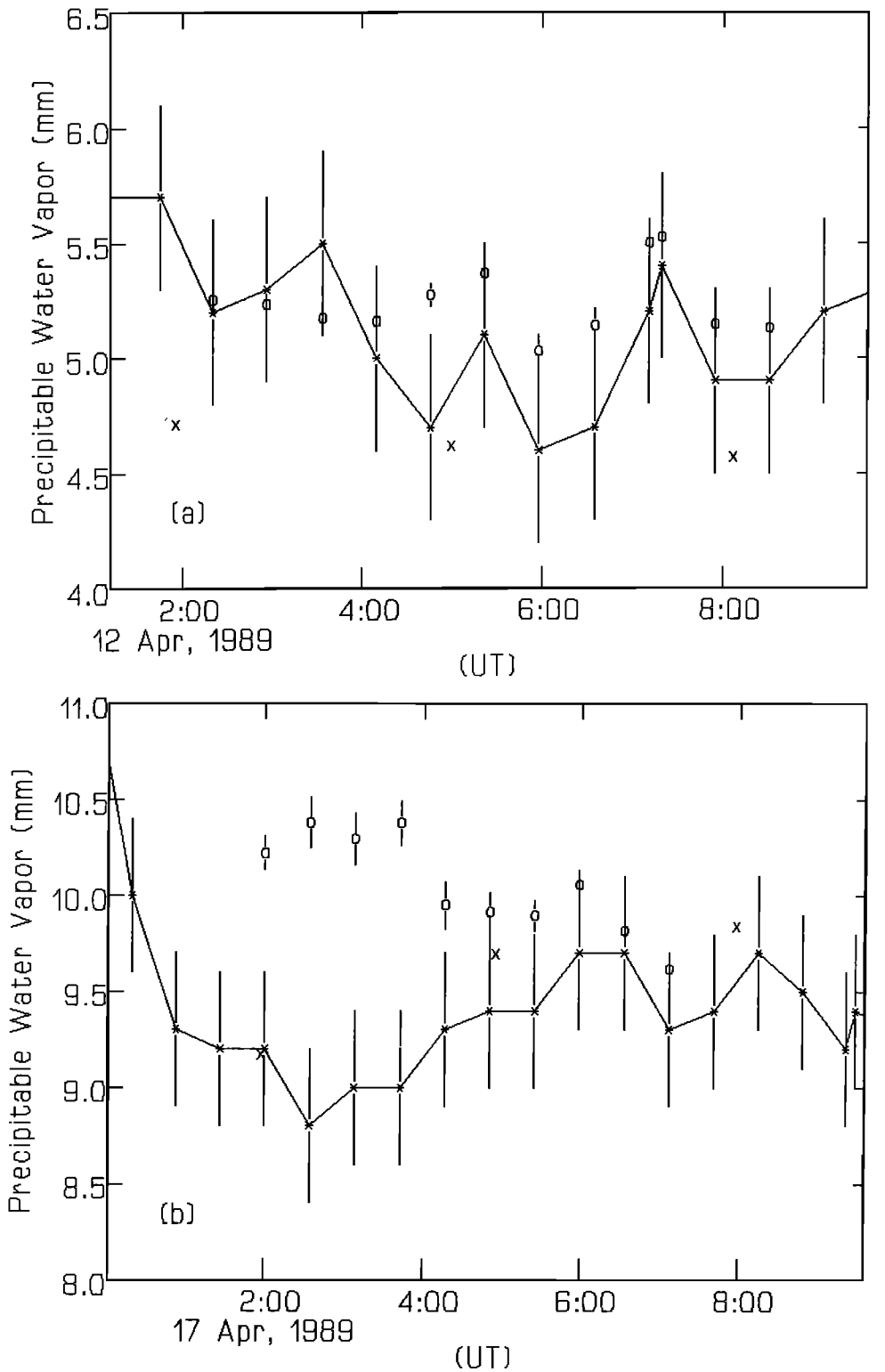

Fig. 9. Integrated precipitable water vapor measurements (in millimeters) at Wallops Island, Virginia, from the lidar (circles) averaged around the times of the WVR measurements (stars) for (*a*) April 11-12, 1989, (*b*) April 16-17, 1989, and (*c*) April 17-18, 1989. The WVR measurements are connected by the line. Integrated precipitable water vapor inferred from the VAISALA radiosondes also are shown (crosses). Error bars represent the random uncertainties on the measurements.

significant portion of the experiment were lost (nights of April 12-16 and the latter portion of the night of April 18, 1989). The reliability of the WVR instrument during the experiment was excellent (data were taken for the whole of the experiment period, but unfortunately not all data were archived). The WVR measurements are the four point averages (spanning a time range of 3.5 min) calculated from the two tip curve results and the two line-of-sight results. The lidar measurements are 2-min averages.

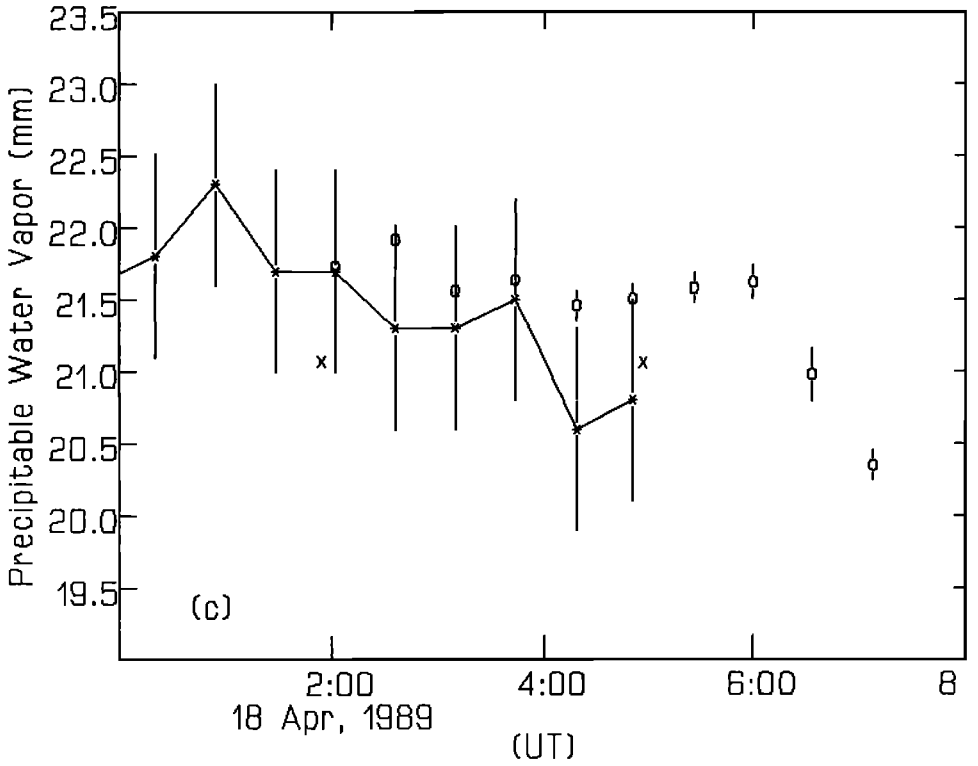

Fig. 9. (continued)

The agreement between the WVR and lidar results is very good for the first period, April 11-12, 1989, Figure 5*a*. The water vapor content for this time period is low (5 mm of precipitable water). A weather front had passed through the area within the previous 24 hours, and the sky was clear, still, and dry. The agreement for the second period, April 16-17, 1989, Figure 5*b*, is not quite as good as for the first period. The moisture content on this night is around 10 mm of precipitable water. However, a

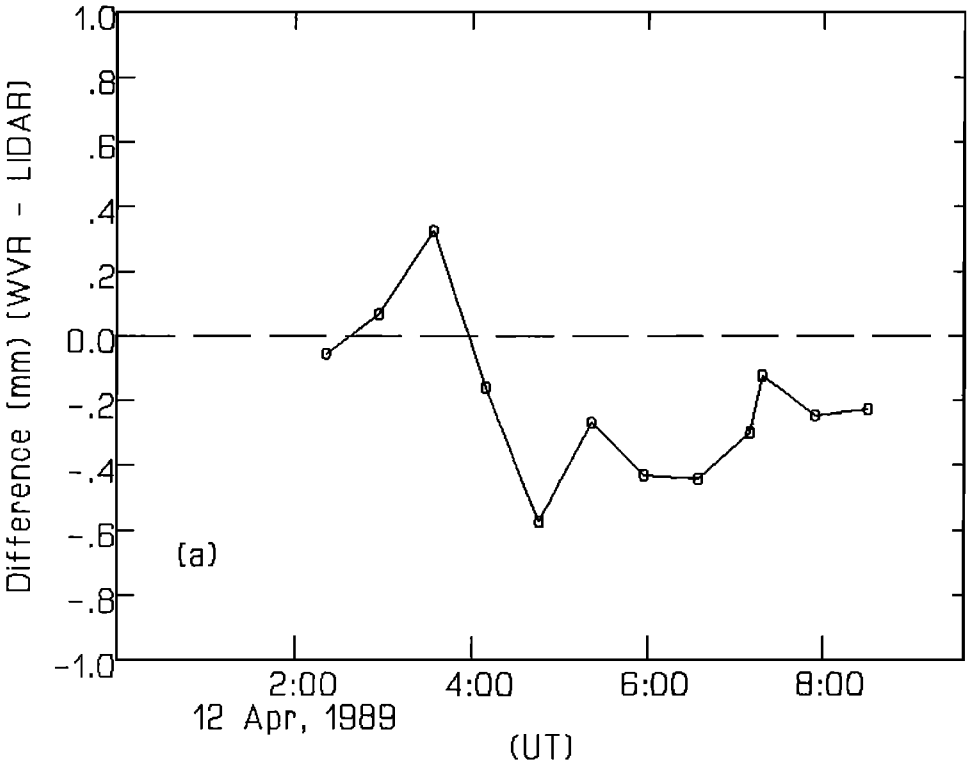

Fig. 10. Differences (in millimeters) between the WVR water vapor measurements and the lidar 30-min averages at Wallops Island, Virginia, for (*a*) April 11-12, 1989, (*b*) April 16-17, 1989, and (*c*) April 17-18, 1989.

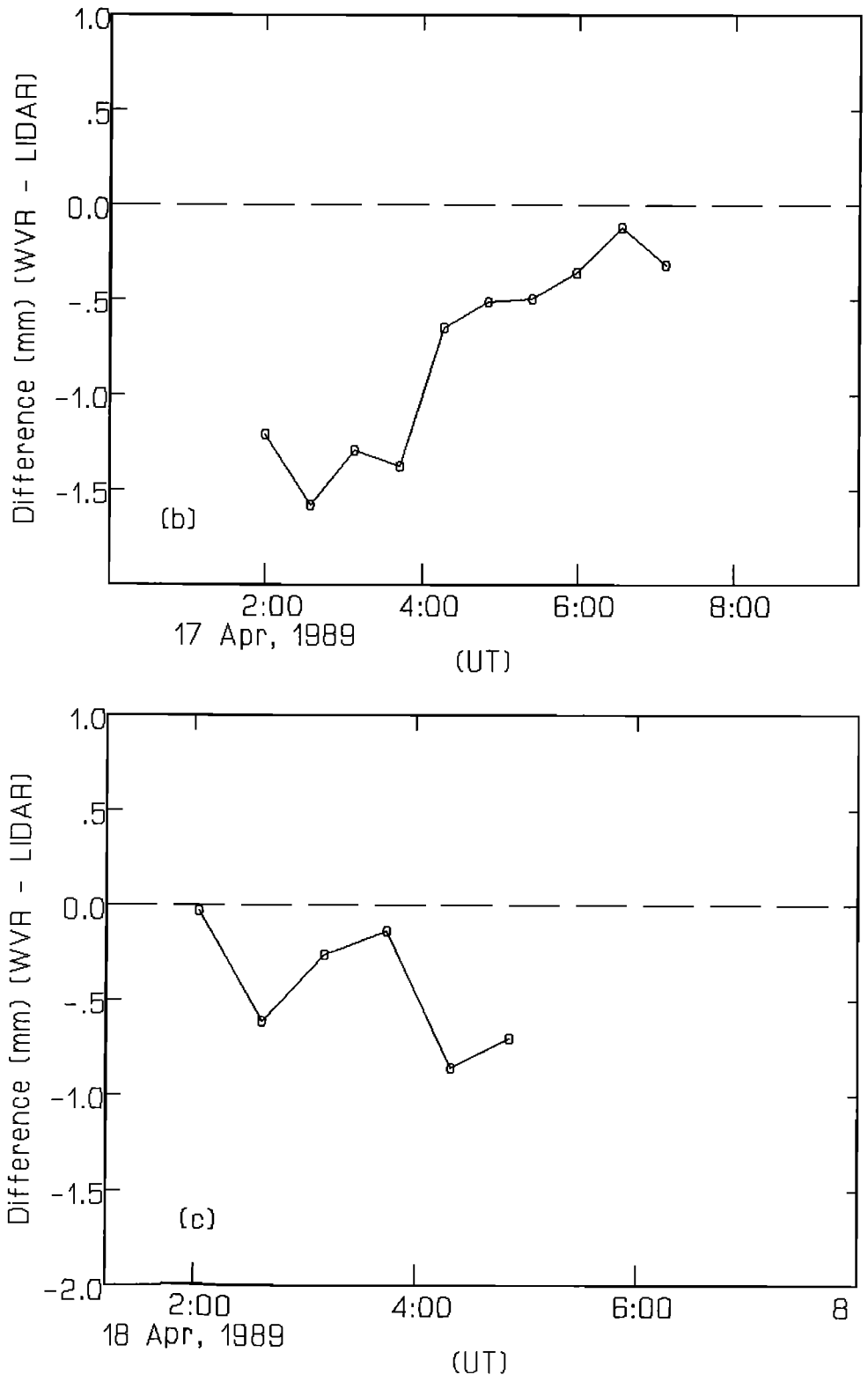

Fig. 10. (continued)

systematic difference between the WVR and the lidar is apparent. The difference between the two instruments decreases through the night. Neither the WVR measurements nor the lidar measurements are anomalous, and the observed trend in the differences is unexplained. The differences are generally small, with the maximum being about 1.6 mm of precipitable water. The night of April 17-18, 1989, was cloudy and significantly more moist (about 21 mm of precipitable water), Figure 5*c*. The WVR measurements have a mean of about 21 mm of precipitable water, whereas the lidar measurements are predominantly at about the 18 mm of precipitable water level. The cloud base height, as inferred from the lidar results, is shown in Figure 6. During periods when clouds are not present, as indicated in Figure 6, the lidar and the WVR measurements are in good agreement. The

lidar is underestimating the water vapor in the presence of clouds because the lidar signal cannot penetrate the clouds. This indicates that a significant amount of water vapor is present above about 4 km (the approximate cloud base height). To emphasize the limitation of the lidar in the presence of clouds, when the lidar results are augmented with the VAISALA radiosonde results above the cloud base, the agreement with the WVR measurements improves (Figure 7). Relative humidity and temperature profiles measured with the VAISALA radiosonde package from the balloon launches at approximately the midpoint of each of the nights are shown in Figures 8*a* and 8*b*. The VAISALA sensor results are shown as the sensor provides readings for relative humidities below 20%. The effect of these clouds can be seen in the relative humidity profile for April 18.

A more quantitative measure of the comparison between the WVR and the lidar was obtained by computing 30-min averages for the lidar results centered around the times of the WVR data. This comparison is shown in Figures 9*a* - 9*c*, and the differences (WVR minus lidar) in Figures 10*a* - 10*c*. The integrated precipitable water vapor results inferred from VAISALA radiosonde measurements for the three periods also are shown with the WVR and lidar measurements in Figures 9*a* - 9*c*. The VAISALA radiosonde results are plotted as this sensor provides relative humidity readings below 20% relative humidity, whereas the AIR and VIZ sensors do not. The mean differences between the WVR and the lidar and standard deviations for the three periods are -0.2 ± 0.2 mm (April 11-12), -0.8 ± 0.5 mm (April 16-17) and -0.4 ± 0.3 mm (April 17-18) (see Table 3). The differences are scattered about these mean values for the nights of April 11-12 and April 17-18 but not for the night of April 16-17, which shows a systematic trend with time. This systematic trend is very evident in Figure 10*b*.

The comparison between the WVR and the lidar measurements for all three time periods is shown in Figure 11. A linear least squares regression solution resulted in a relation between the WVR and lidar precipitable water vapor of $PW_{wvr} = 0.992(PW_{lidar})-0.37$ for the 28 data pairs. A high correlation (r = 0.998) between the WVR and lidar measurements was obtained for the whole data set.

The only common element in the comparison between the WVR and lidar measurements is that ultimately the calibration for both methods relies upon radiosonde data, albeit in different fashions. The lidar uses radiosonde data to provide the absolute mixing ratio scale for the profiles. The WVR uses radiosonde data to determine sets of retrieval coefficients for the moisture

TABLE 3. Integrated Water Vapor Measurements in Millimeters

	Summary		
Date	April 11-12	April 16-17	April 17-18
Number of pairs	12	10	6
Total precipitable vapor (WVR)	5	10	21
Mean difference[a]	-0.2	-0.8	-0.4
Standard deviation[a]	0.2	0.5	0.3
Bias error (WVR)	0.8	0.9	1.4
Random error (WVR)	0.4	0.4	1.3
Total error (WVR)	0.9	1.0	1.9

Regression results with WVR and lidar: $PW_{wvr} = m(PW_{lidar}) + c$; slope ($m$), 0.992 mm/mm; intercept (c), -0.37 mm; correlation coefficient, 0.998; number of pairs, 28.

[a] Difference is (WVR minus lidar).

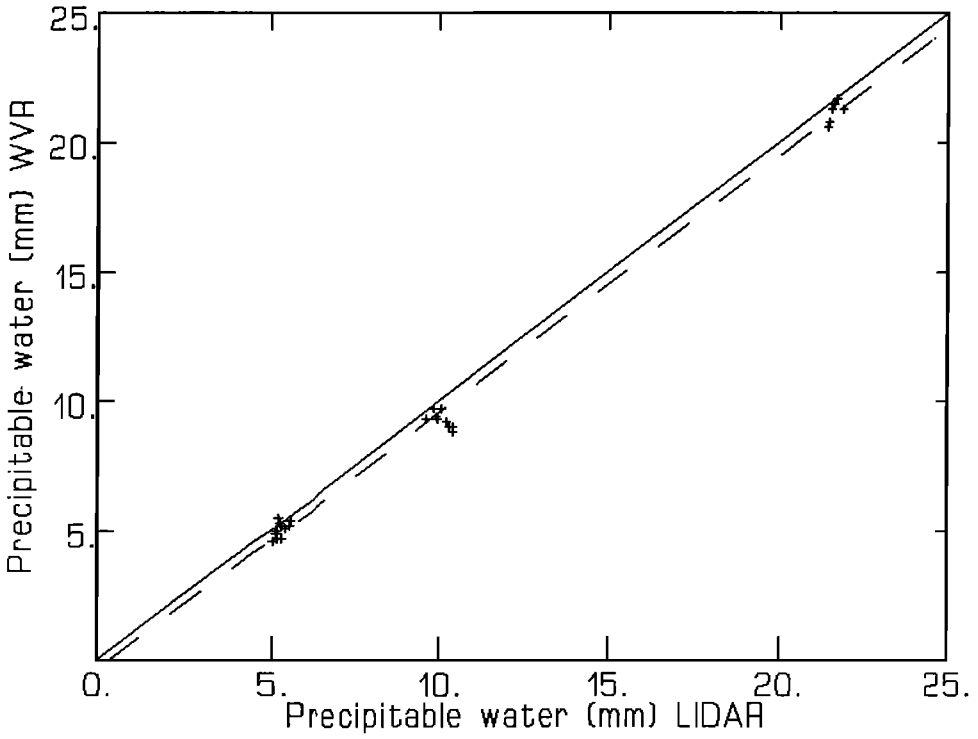

Fig. 11. Scatterplot of the lidar and WVR integrated precipitable water vapor measurements. The least squares regression line, $PW_{wvr} = m(PW_{lidar})+c$, is shown (dashed line) as well as the $PW_{wvr} = PW_{lidar}$ line (solid line).

measurements. In its normal operating mode the WVR uses long term averages of radiosonde data to provide general retrieval coefficients. The radiosonde data cover a specific time period (e.g., 1979-1982 for the coefficients used here), but the retrieval coefficients derived from these data are applied to all other times. On the other hand, the radiosonde data used to calibrate the lidar system are taken simultaneously with the lidar measurements (e.g. the lidar system here was calibrated with data from radiosondes launched every 3 hours during the experiment). The main focus of this study was to determine the performance of the WVR under normal, routine Crustal Dynamics Project operating conditions. These procedures use time-averaged retrieval coefficients for the moisture measurements, and because a follow-on experiment is planned for late 1991 and because of the short time span of data available for this intercomparison, the question of the difference in using time-averaged retrieval coefficients and site specific, simultaneously determined retrieval coefficients has not been directly addressed in this study, although the importance of the retrieval coefficients is recognized. The follow-on experiment will concentrate on validation of the results of this study and on the issue of the suitability of time-averaged or "instantaneous" retrieval coefficients and the uncertainties associated with each. Coupled to this follow-on experiment is an analysis of the uncertainties in the radiosonde measurements of temperature, pressure, and relative humidity (see M. N. England et al., Atmospheric Moisture Measurements: Are All Radiosondes Equal? A Microwave Radiometer-Radiosonde Comparison, submitted to IEEE Trans. Geosci. Remote Sens., 1991).

Because the agreement between the two moisture-measuring techniques is good through a variety of meteorological conditions, the conclusion is that the WVR measurements are accurate estimates of the integrated water vapor content of the atmospheric column being observed. The excellent agreement between these independent measurement techniques gives confidence that the WVR is capable of accurately measuring the sky brightness temperatures and from these deriving the extra "wet" signal path delay and the moisture content of the troposphere.

Acknowledgments. A word of thanks is owed to the Science Review Board at Interferometrics Inc. for their useful reviews, especially Clara Kuehn, whose comments and suggestions greatly improved both the presentation and the content of this paper, and to the reviewers who contributed useful comments. We also would like to thank Frank Schmidlin for the radiosonde data, the staff at Wallops Island, Virginia, for the balloon launches, Al Wu, Dave Sims, and Mark Hitch of Bendix Field Engineering Corp., Columbia, Maryland, for their support of the J03 instrument, and the staff at the NASA/GSFC Crustal Dynamics Project.

REFERENCES

Askne, J., G. Elgered, H. Nordius, G. Skoog, E. Winberg, A. Hagard, E. Andersson, N. Gustafsson, J. Svensson, and I. Carlsson, The ONSAM experiment: Remote sensing techniques for vertical sounding of the atmosphere, *J. Atmos. Ocean Technol., 4,* 180, 1987.

Becker, G.E., and S. H. Autler, Water vapor absorption of electromagnetic radiation in the centimeter wavelength range, *Phys. Rev., 70,* 300, 1946.

Brousaides, F.J., The radiosonde hygristor and low relative humidity measurements, *Bull. Am. Meteorol. Soc., 56,* 229, 1975.

Clark, T.A., et al., Precision geodesy using the Mark-III very-long-baseline interferometer system, *IEEE Trans. Geosci. Remote Sens., GE-23,* 438, 1985.

Davis, J.L., T.A. Herring, I.I. Shapiro, A.E.E. Rogers, and G. Elgered, Geodesy by radio interferometry: Effects of atmospheric modeling errors on estimates of baseline length, *Radio Sci., 20,* 1593, 1985.

Dicke, R.H., R. Beringer, R.L. Kyhl, and A.B. Vane, Atmospheric absorption measurements with a microwave radiometer, *Phys. Rev., 70,* 340, 1946.

Elgered, G., B.O. Ronnang, J.I.H. Askne, Measurements of atmospheric water vapor with microwave radiometry, *Radio Sci., 17,* 1258, 1982.

Elgered, G., J.L. Davis, T.A. Herring, and I.I. Shapiro, Geodesy by radio interferometry: Water vapor radiometry for estimation of the wet delay, *J. Geophys. Res., 96,* 6541, 1991.

Gary, B.L., and S.J. Keihm, Path delay retrieval coefficients for use with water vapor radiometers operating at sites of the Crustal Dynamics Project, Interim Report, Jet Propul. Lab., Pasadena, Calif, 1986.

Gary, B.L., S.J. Keihm, and M.A. Janssen, Optimum strategies and performance for the remote sensing of path delay using ground-based microwave radiometers, *IEEE Trans. Geosci. Remote Sens., GE-23,* 479, 1985.

Gipson, J.M., and G.L. Lundqvist, The effect of random and systematic errors on the sensitivity and precision of water vapor radiometers, NASA Crustal Dynamics Internal Report, Goddard Space Flight Center, Greenbelt, Md, 1986.

Goldstein, H., Attenuation by condensed matter, in *Propagation of Short Radio Waves,* edited by D.E. Kerr, p. 671, McGraw-Hill, New York, 1951.

Haltiner, G.J., and F.L. Martin, *Dynamical and physical meteorology,* McGraw-Hill Book Company, Inc., New York, 1957.

Heggli, M., R.M. Rauber, and J.B. Snider, Field evaluation of a dual-channel microwave radiometer designed for measurements of integrated water vapor and cloud liquid water in the atmosphere, *J. Atmos. Oceanic Technol., 4,* 204, 1987.

Hogg, D.C., F.O. Guiraud, J.B. Snider, M.T. Decker, and E.R. Westwater, A steerable dual-channel microwave radiometer for measurement of water vapor and liquid in the troposphere, *J. Appl. Meteorol., 22,* 789, 1983.

Janssen, M.A., A new instrument for the determination of radio path delay variations due to atmospheric water vapor, *IEEE Trans. Geosci. Remote Sens., GE-23,* 485, 1985.

Johansson, J.M., G. Elgered, J.L. Davis, Geodesy by radio interferometry: Optimization of wet path delay algorithms using microwave radiometer data, *Res. Rep. No. 152,* Chalmers Univ. of Technol., Goteborg, Sweden, 1987.

Kaiser, J.F., and W.A. Reed, Data smoothing using low-pass digital filters, *Rev. Sci. Instrum., 48,* 1447, 1977.

Liebe, H.J., and D.H. Layton, Millimeter-wave properties of the atmosphere: Laboratory studies and propagation modeling, *Rep. 87-224,* Natl. Telecommun. and Inf. Admin., Boulder, Colo., 1987.

Melfi, S.H., Remote measurements of the atmosphere using Raman scattering, *Appl. Opt., 11,* 1605, 1972.

Melfi, S.H., and D. Whiteman, Observation of lower-atmospheric moisture structure and its evolution using a Raman lidar, *Bull. Am. Meteorol. Soc., 66,* 1288, 1985.

Melfi, S.H., D. Whiteman, and R.A. Ferrare, Observation of atmospheric fronts using Raman lidar moisture measurements, *J. Clim. Appl. Meteorol., 28,* 789, 1989.

Resch, G.M., Water vapor - The wet blanket of microwave interferometry, in *Atmospheric Water Vapor,* edited by A. Deepak, T.D. Wilkerson, and L.H. Ruhnke, p. 265, Academic, San Diego, Calif., 1980.

Resch, G.M., Inversion algorithms for water vapor radiometers operating at 20.7 and 31.4 GHz, *TDA Prog. Rep. 42-76,* Jet Propul. Lab., Pasadena, Calif, 1983.

Resch, G.M., M.C. Chavez, N.I. Yamane, K.M. Barbier, R.C. Chandlee, Water vapor radiometry research and development phase: Final report, *Pub. 85-14,* Jet Propul. Lab., Pasadena, Calif., 1985.

Robinson, S.E., The profile algorithm for microwave delay estimation from water vapor radiometer data, *Radio Sci., 23,* 401, 1988.

Rosenkranz, P.W., Interface coefficients for overlapping oxygen lines in air, *J. Quant. Spectrosc. Radiat. Transfer, 39,* 287, 1988.

Shapiro, I.I., Estimation of astrometric and geodetic parameters, in *Methods of Experimental Physics,* Vol. 12C, edited by M.L. Meeks, p. 264, Academic, San Diego, Calif., 1976.

Van Vleck, J.H., The absorption of microwaves by uncondensed water vapor, *Phys. Rev., 71,* 425, 1947.

Wade, C.G., and D.E. Wolfe, Performance of the VIZ carbon hygristor in a dry environment, paper presented at 12th Conference on Weather Analysis and Forecasting, Amer. Meteorol. Soc., Monterey, Calif., 1989.

Westwater, E.R., An analysis of the correction of range errors due to atmospheric refraction by microwave radiometric techniques, *Tech. Rep. IER 30-ITSA30,* Environ. Sci. Serv. Admin., Boulder, Colo., 1967.

Westwater, E.R., Ground-based determination of low-altitude temperature profiles by microwaves, *Mon. Weather Rev., 100,* 15, 1972.

Westwater, E.R., The accuracy of water vapor and cloud liquid determination by dual-frequency ground-based microwave radiometry, *Radio Sci., 13,* 677, 1978.

Westwater, E.R., M.J. Falls, and I.A. Popa Fotina, Ground-based microwave radiometric observations of precipitable water vapor: A comparison with ground truth from two radiosonde observing systems, *J. Atmos. Oceanic Technol., 6,* 724, 1989.

Whiteman, D.N., S.H. Melfi, and R.A. Ferrare, Raman lidar system for the measurement of water vapor and aerosols in the Earth's atmosphere, *Appl. Opt.,* in press, 1991.

D. N. Whiteman, Laboratory for Terrestrial Physics, Code 924.0, NASA/Goddard Space Flight Center 20771.

T. A. Clark, Laboratory for Terrestrial Physics, Code 926.9, NASA/Goddard Space Flight Center 20771.

Martin N. England, IUE Observatory, Computer Sciences Corporation, Code 684.9, NASA/Goddard Space Flight Center, Greenbelt, MD 20771.

R. A. Ferrare and S. H. Melfi, Laboratory for Atmospheres, Code 917.0, NASA/Goddard Space Flight Center, Greenbelt, MD 20771.

(Received January 8, 1991;
revised June 4, 1991;
accepted July 17, 1991.)